

Translation-invariant functional clustering on COVID-19 deaths adjusted on population risk factors

Amay SM Cheam¹, Marc Fredette², Matthieu Marbac³, and Fabien Navarro⁴

^{1,2}HEC Montreal, Quebec, Canada

^{3,4}Univ. Rennes, Ensai, CNRS, CREST - UMR 9194, F-35000 Rennes, France

December 22, 2024

Abstract

The COVID-19 pandemic has taken the world by storm with its high infection rate. Investigating its geographical disparities has paramount interest in order to gauge its relationships with political decisions, economic indicators, or mental health. This paper focuses on clustering the daily death rates reported in several regions of Europe and the United States over eight months. Several methods have been developed to cluster such functional data. However, these methods are not translation-invariant and thus cannot handle different times of arrivals of the disease, nor can they consider external covariates and so are unable to adjust for the population risk factors of each region. We propose a novel three-step clustering method to circumvent these issues. As a first step, feature extraction is performed by translation-invariant wavelet decomposition which permits to deal with the different onsets. As a second step, single-index regression is used to neutralize disparities caused by population risk factors. As a third step, a nonparametric mixture is fitted on the regression residuals to achieve the region clustering. Supplementary materials for this article, including a standardized description of the materials available for reproducing the work, are available online.

Keywords: Functional data; Mixture models; Semiparametric models; Single-index regression; Wavelets;

1 Introduction

In March of 2020, the World Health Organization (WHO) declared pandemic status for the novel coronavirus SARS-Cov-2, denoted COVID-19, indicating that it has reached a critical level of spread and severity worldwide. The global nature of COVID-19 pandemic has resulted in plenty of heterogeneity of the data, aggravated further by lack of prior knowledge or coordinated mitigation strategies which impeded research efforts. For instance, the assumption that the first occurrence emerged concurrently everywhere is improper. Additionally, the number of confirmed cases depends on the amount of tests that are being performed in a region. Hence, a region that has tested very few people can only report very few confirmed cases. Alternatively, the number of COVID-19 deaths is more systematically recorded: countries are asked to follow the ‘cause of death’ classifications from the WHO’s International Classification of Diseases guidelines (World Health Organization, 2016). Though each country is responsible to provide their own guidance on how and when COVID-19 deaths should be recorded, this metric remains more reliable. Undoubtedly, the rapid propagation of this acute infectious respiratory disease has posed governmental challenges. Government responses to contain the virus’s spread were multiple (social distancing, travel restrictions, lockdowns, etc.) and their efficiency needs to be investigated. To better understand this virus, it is profoundly useful to cluster regions similarly affected by COVID-19.

In this paper, we focus on clustering regions of the European Union (EU) and the United States of America (USA) based on the daily COVID-19 deaths recorded over eight months. Previous investigations of geographical disparities of COVID-19 (Tang et al., 2020; Chen et al., 2020) only focus on specific geographical regions (*e.g.*, USA). When considering regions of Europe and North America, a difficulty arises: COVID-19 outbreaks started at different times. The misalignment of the first occurrence between regions should not be neglected, whether between continents or within a country. Another problem to acknowledge is that the mortality occurs at different rates under different population risk factors (Williamson et al., 2020). Hence the necessity to adjust these region-specific risk factors is intrinsic to allow regions to be compared fairly. Furthermore, by adjusting the population

risk factors, we are able to detect regions more susceptible to COVID-19 and perhaps identify the disparity factors between clusters. For instance, it allows for a retrospective assessment of the effectiveness and the quality of government responses, a concurrent analysis of the economic indicators, and a prospective perception of mental health during this unprecedented period.

Traditionally, clustering may be achieved through finite mixture models (McLachlan and Peel, 2004). When the family of distributions for each cluster is unknown, nonparametric mixtures can be considered to avoid unjustified parametric assumptions (Chauveau et al., 2015). A classical approach among these methods is to define the density of each mixture component as a product of univariate densities (Hall and Zhou, 2003; Kasahara and Shimotsu, 2014). The data we analyze are functional and thus raise the problem of data dimension (Ferraty and Vieu, 2006; Ramsay and Silverman, 2007). To circumvent the curse of dimensionality, many model-based clustering approaches approximate the observed functions in some functional basis then perform clustering on the coefficients related to the basis (see the review of Jacques and Preda (2014) or Cheam and Fredette (2020)). For instance, Bouveyron et al. (2015) proposed to approximate the curves into a Fourier basis expansion coefficients and then perform clustering on the obtained coefficients with a Gaussian mixture. Alternatively, feature extraction can also be accomplished via an orthogonal wavelet basis (Antoniadis et al., 2013).

In this article, we propose a novel three-step approach that circumvents the issues of the region clustering based on COVID-19 dataset: the varying times of arrivals of the virus and the need to incorporate the population risk factors. This approach is named *Clustering Regression residuals of Features given by Translation Invariant Wavelets* (CRFTIW). The first step of CRFTIW consists of feature extraction using a multiscale approach based on translation-invariant (TI) wavelets (Coifman and Donoho, 1995), which allows the shifted onsets of COVID-19 to be tackled by avoiding any pre-processing step for curve alignment (see Wang and Gasser (1997) and the references cited in Jacques and Preda (2014, Section 2.3)). The objective to construct clusters that are invariant to time-shifts is somewhat dif-

ferent from conventional clustering in that it permits us to answer slightly different scientific questions about the data. Standard clustering (no time-shifts) will identify regions that peak at the same period, while TI clustering recovers regions that react in similar behavior patterns that unravel across time. The features are defined as the logarithm of the norm of the TI wavelet coefficients at each scale. The second step of **CRFTIW** integrates the population characteristics with a single-index regression of the features on the population risk factors. This approach has the benefits of the nonparametric regression but does not suffer from the curse of dimensionality. Moreover, the empirical likelihood (Qin and Lawless, 1994; Owen, 2001) permits the significance of the estimators to be investigated (Zhu and Xue, 2006), even when dependency between observations occurs (Du Roy de Chaumaray et al., 2020). We show that the residuals of the regression preserve the cluster information. As the third step of **CRFTIW**, clustering of the regions is achieved by fitting a nonparametric mixture on the regression residuals. The only assumption made at this step is to define the density of each component as a product of univariates densities.

The remainder of this article is organized as follows. Section 2 presents the data. Section 3 defines the new approach **CRFTIW**. Section 4 illustrates, with numerical experiments, the relevance of **CRFTIW**. In Section 5, we analyze the geographical disparities of the COVID-19 by investigating the regression coefficients, by describing the clusters according to the diseases and by illustrating the use of the clusters to investigate policy strategies. Section 6 presents some concluding remarks.

2 Description of the data

For this ongoing COVID-19 dataset, we consider $n = 78$ regions between two continents: the 26 countries within the EU plus the United Kingdom and the 50 states of the USA plus the District of Columbia. There are differences in time of arrival of the peak death rates between regions. This is illustrated by Figure 1 which shows that New Hampshire and Pennsylvania have noticeably more delayed peaks than France and United Kingdom.

Our focus is on the curve $W_i = (W_{i(1)}, \dots, W_{i(T)})^\top$ recording the daily rate of the number

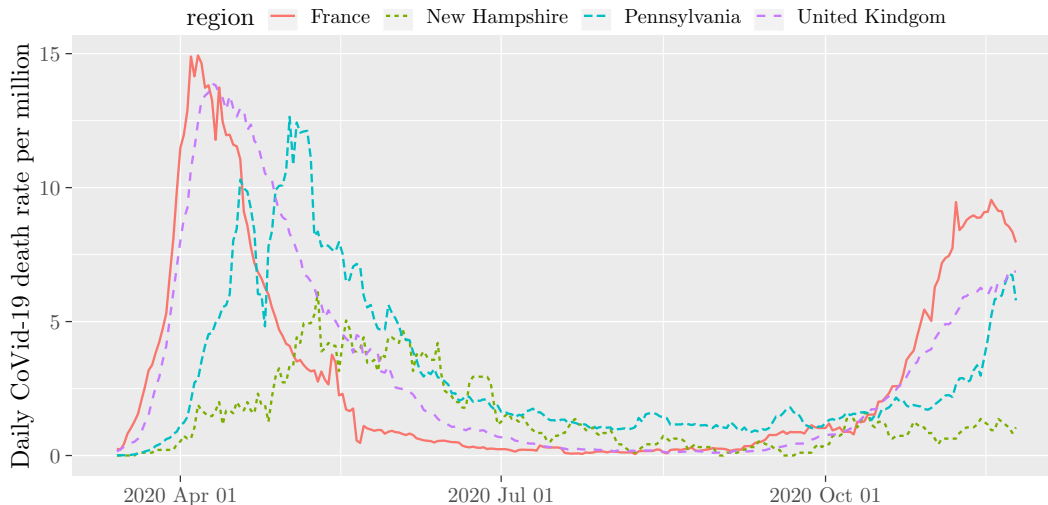


Figure 1: Illustration of different arrivals of the COVID-19 among the different regions.

of deaths per million people in each region i for a total of $T = 256$ days (between March 14 to November 24, 2020, inclusively), where $W_{i(t)}$ denotes the death rate recorded for region i at time t . Data were extracted from the Center for Systems Science and Engineering at Johns Hopkins’ Github repository (Badr et al., 2020) and a 7-day moving average has been performed due to the discrepancy of the data recorded by each region. For instance, this can account for days in the week where data may not be available, such as weekends.

Early findings suggested that differences in COVID-19 disease prevalence and severity may be associated with certain risk factors (Williamson et al., 2020). For each region i , we store in $X_i \in \mathbb{R}^4$ the indicator of four population risk factors based on WHO statements: *Overweight*, *Diabetes*, *Pulmonary* and *Kidney*. *Overweight* indicates the crude prevalence of overweight adults defined by the body mass index (Kang et al., 2020) while *Diabetes* indicates the age-adjusted prevalence of diabetes (Barron et al., 2020; Holman et al., 2020). Both data, expressed as a percentage of the population and recorded in 2016, can be accessed from the Center for Disease Control and Prevention (2020) and World Health Organization (2020), respectively for the US and the EU. *Pulmonary* indicates the prevalence of chronic obstructive pulmonary disease (COPD). Although Attaway et al. (2020) found no significant increases in the rate of COVID-19 between COPD and non-COPD patients, the authors

noticed significantly higher rates of hospitalization, ICU admissions and invasive mechanical ventilation in COPD patients. Finally, *Kidney* indicates the prevalence of chronic kidney disease. Williamson et al. (2020) demonstrated that patients with severe form of chronic kidney disease have higher rates of COVID-19-related deaths than the other known high-risk groups. *Pulmonary* and *Kidney* are available on the Global Burden of Disease Collaborative Network (2020)’s database, were age-adjusted and given in percentages for 2019. For ease of interpretation, the population risk factors have been scaled.

3 Method

3.1 Outline of the three-step method

The daily COVID-19 death curves of the n regions W_1, \dots, W_n are supposed to independently arise from L different clusters. The cluster membership of region i is defined by the latent variable $Z_i = (Z_{i1}, \dots, Z_{iL})^\top$ where $Z_{i\ell} = 1$ if region i belongs to cluster ℓ and $Z_{i\ell} = 0$ otherwise. The model assumes that, conditionally on the cluster ℓ , each W_i is defined as a product between a noisy version of δ_i -lagged values of an unobserved curve u_ℓ and the effect of the population risk characteristics $\mu(X_i) > 0$, where X_i denotes population risk factors of region i and where we set $\mathbb{E}[\mu(X_i)] = 1$, for identifiability reasons. The deterministic functions u_ℓ do not depend on the covariates X_i . Moreover the noises $\varepsilon_{i\ell}$ and the covariates X_i are independent. Thus, given the cluster membership and the population risk factors of region i , we have

$$W_i = \sum_{\ell=1}^L z_{i\ell} \mu(x_i) (u_\ell^{(\delta_i)} + \varepsilon_{i\ell}^{(\delta_i)}), \quad (1)$$

where $u_\ell^{(\delta_i)}$ and $\varepsilon_{i\ell}^{(\delta_i)}$ are δ_i -lagged versions of u_ℓ and $\varepsilon_{i\ell}$, and the distribution of each $\varepsilon_{i\ell}$ follows a centered distribution having a finite variance defined by the density f_ℓ (i.e., $\mathbb{E}_{f_\ell}[\varepsilon_{i\ell}] = 0$ and $\mathbb{E}_{f_\ell}[\varepsilon_{i\ell}^2] < \infty$). Thus, the conditional distribution of W_i given $X_i = x_i$ is defined by the density

$$f(w_i | x_i) = \sum_{\ell=1}^L \pi_\ell f_\ell \left(\frac{w_i}{\mu(x_i)} - u_\ell^{(\delta_i)} \right), \quad (2)$$

where $\pi_\ell > 0$ is the proportion of cluster ℓ with $\sum_{\ell=1}^L \pi_\ell = 1$.

Despite the model defined by (2) permitting a clustering of the regions based on the daily COVID-19 death curves with respect to the population risk factors, the estimation the multivariate densities f_ℓ is highly complex. Thus, we achieve the clustering with the following three-step approach:

1. Perform feature extraction of the daily COVID-19 death curves W_i to obtain $Y_i \in \mathbb{R}^{J+1}$ using TI wavelets (see Section 3.2).
2. Fit single-index regressions of the features Y_i on the population risk factors X_i and consider the residuals $\hat{\xi}_i \in \mathbb{R}^{J+1}$ (see Section 3.3).
3. Use the nonparametric mixture to cluster the regions based on the residuals $\hat{\xi}_i$ (see Section 3.4).

This approach is relevant since the specific feature extraction reduces the dimension, permits us to deal with lagged values and keeps the main cluster information. Moreover, the single-index regression keeps the cluster information of the features, allows for adjustment on population risk factors, and provides meaningful parameters used for detecting protective or compounding effects of the population characteristics and odd ratios.

3.2 Feature extraction and time misalignment

A wavelet basis is a set of functions obtained as translations and dilatations of two specific functions: a scaling function denoted by ϕ and a mother wavelet denoted by ψ . For the purpose of this paper, we use Daubechies wavelets and in particular the Symmlet family. Such wavelets are optimal in the sense that they have minimal support for a given number of null moments. We present the essentials below; more details can be found in Daubechies (1992) or Mallat (2008).

The decomposition of the observations in a given wavelet basis is defined by

$$W_i(t) = \alpha_{i,0,0}\phi_{0,0}(t) + \sum_{j=0}^{J-1} \sum_{k=0}^{2^j-1} \beta_{i,j,k}\psi_{j,k}(t), \quad t \in [1, T].$$

with $J = \log_2(T)$, $\phi_{j,k}(t) = 2^{j/2}\phi(2^j t - k)$, $\psi_{j,k}(t) = 2^{j/2}\psi(2^j t - k)$, $\alpha_{i,0,0} \approx \sqrt{T} \int_1^T W_i(t)\phi_{0,k}(t)dt$ and $\beta_{i,j,k} \approx \sqrt{T} \int_1^T W_i(t)\psi_{j,k}(t)dt$ are the empirical wavelet coefficients of the i th individual. A discrete wavelet transform (DWT) corresponds to the computation of these coefficients. In practice, a fast wavelet decomposition and reconstruction algorithm can be computed using the algorithm proposed by Mallat (1989) (in only $\mathcal{O}(T)$ operations). As mentioned in the introduction, a simple shift in the observed function will potentially result in a significant change in the DWT. Since we use the latter for feature extraction and the observed curves can start at different times, such behavior is not suitable.

In the TI case, we consider the fast translation-invariant discrete wavelet transform (TIDWT) developed by Coifman and Donoho (1995), in a denoising framework. The main difference with the orthogonal case is that the dictionary is now a tight frame instead of an orthonormal basis (see (Mallat, 2008, Chapter 5)) and the number of coefficients per scale is no longer dyadic but of length T (see Coifman and Donoho (1995) for more details). This wavelet transform is called translation-invariant since the whole dictionary is invariant under circular translation. More precisely, for a vector w of size T , let S_h denotes the circulant shift by h defined by $(S_h w)(t) = w(t + h)$ modulo T . As in the traditional case, TIDWT is calculated by a series of decimation and filtering operations, only the additional circulant shift S_h is added and the corresponding wavelet dictionary is obtained by sampling the locations more finely (*i.e.*, one location per sample point). TIDWT consists of calculating the DWT of the shifted data for each shift $h \in \{0, \dots, T - 1\}$. Coifman and Donoho (1995) propose an algorithm to perform this transformation in $\mathcal{O}(T \log_2 T)$ operations (we used the R package **rwavelet** which provides an implementation Navarro and Chesneau (2020)). The invariance property of their construction is formally expressed in terms of the circulant matrix containing the wavelet coefficients (see (Coifman and Donoho, 1995, eq. (3))). In other words, for a curve W_i translated by h the wavelet coefficients at each scale will be the same up to some permutation. Thus the norm of the latter is preserved scale by scale.

The redundancy of TIDWT makes it possible to detect the presence of hidden information such as stationary or non-stationary patterns as well as their location, making it

particularly suitable for clustering purposes. This type of invariant representation has been exploited in many applications (such as denoising Coifman and Donoho (1995) or texture image classification and segmentation Unser (1995)). In addition, the use of wavelets allows to compress the information contained in the time series into a small number of wavelet coefficients. Following Antoniadis et al. (2013), we characterize each time series by the vector of the energy contribution of their wavelet coefficients at each scale with the difference that the coefficients are calculated by TIDWT instead of DWT. This extension is possible because the expansion being in a *tight frame*, the norm is also conserved (see (Mallat, 2008, Chapter 11) for more details). More precisely, using Parseval’s identity, we have

$$\|W_i\|_2^2 = 2^{-J} \sum_{k=0}^{T-1} \alpha_{i,0,k}^2 + \sum_{j=1}^J 2^{-j} \sum_{k=0}^{T-1} \beta_{i,j,k}^2 = 2^{-J} \|\theta_{i0}\|_2^2 + \sum_{j=1}^J 2^{-j} \|\theta_{ij}\|_2^2, \quad (3)$$

where $\theta_{ij} = (\alpha_{i,0,0}, \dots, \alpha_{i,0,T-1}, \beta_{i,j,0}, \dots, \beta_{i,j,T-1})^\top$ and the factor 2^{-j} is used to compensate for the redundancy of this representation. Thus, denoting by y_{ij} the log total norm at scale j for the i th individual, we have

$$y_{ij} = \ln(\|\theta_{ij}\|_2), \quad \forall j = 0, \dots, J, \quad i = 1, \dots, n. \quad (4)$$

Clustering will therefore be carried out on the basis of the log norm of the TI wavelet coefficients at each scale. Thus, this criterion is not sensitive to the origin of the curves, so it seems relevant given the nature of the data motivating this work.

3.3 Adjustment on the population risk factors

In this section, we consider the regressions of the features extracted by the wavelet decomposition on the population risk factors. The following lemma shows that the noises of these regressions retain the cluster information given by the daily COVID-19 death curves and permit the information of the population risk factors to be considered in the clustering procedure. Note that the same nonparametric function is used for the regression of each feature (*i.e.*, $j = 0, \dots, J$). Thus, the lemma shows how the regression function is estimated based on the $n \times (J + 1)$ observations.

Lemma 1. *Let data arise from (2) and features are defined by (4). Defines the noise of the regression $\xi_i = (\xi_{i1}, \dots, \xi_{id})^\top$ for $j = 0, \dots, J$ as*

$$y_{ij}^* = m(x_i) + \xi_{ij}, \quad (5)$$

with

$$\mathbb{E}[m(X_i)] = 0 \text{ and } \mathbb{E}[\xi_{ij}] = 0,$$

where x_i and ξ_{ij} are independent, $y_{ij}^* = y_{ij} - \Delta_j$, $m(x_i) = \ln \mu(x_i) - \mathbb{E}[\ln \mu(X_i)]$, $\Delta_j = \mathbb{E}[\ln \mu(X_i)] + \sum_{\ell=1}^L \pi_\ell \mathbb{E}[\frac{1}{2} \ln \|v_{\ell j} + \varepsilon_{i\ell j}^*\|_2^2]$, and $v_{\ell j}$ and $\varepsilon_{i\ell j}^*$ are the features of u_ℓ and $\varepsilon_{i\ell}$, respectively (their formal definition is given in the proof of the lemma presented in Appendix).

Then, the noises ξ_i follow a mixture model with latent variable Z_i defined by the density

$$g(\xi_i) = \sum_{\ell=1}^L \pi_\ell g_\ell(\xi_i - \lambda_\ell),$$

where $\lambda_\ell = (\lambda_{\ell 1}, \dots, \lambda_{\ell J})^\top$, $\lambda_{\ell j} = \mathbb{E}[\frac{1}{2} \ln \|v_{\ell j} + \varepsilon_{i\ell j}^*\|_2^2] - \Delta_j + \mathbb{E}[\ln \mu(X_i)]$ and g_1, \dots, g_ℓ are densities of centered distributions.

We consider the single-index regression defined by

$$m(x_i) := \nu(x_i^\top \gamma). \quad (6)$$

This semiparametric approach is flexible, and avoids the assumptions of the parametric approaches that can be violated and the curse of dimensionality of the full nonparametric approaches. The parameter of the index γ permits population characteristics having a protective or compounding effect to be detected. Moreover, considering two sets of covariates X_i and $X_{i'}$, the difference $\nu(X_i^\top \gamma) - \nu(X_{i'}^\top \gamma)$ can be interpreted as the logarithm of an odd ratio.

The single-index approach requires a methodology for estimating γ and m , with m being in a function space. A common approach, that avoids a simultaneous search involving an infinite-dimensional parameter, is the profiling (Severini and Wong, 1992; Liang et al., 2010), which defines $\nu(x_i^\top \gamma) := \nu_\gamma$ with

$$\nu_\gamma(t) = \mathbb{E}[Y_{ij}^* | X_i^\top \gamma = t], \quad j \in \{0, \dots, J\} \text{ and } t \in \mathbb{R}. \quad (7)$$

Hence, one expects that, for each x_i , the true value of the parameter, denoted by γ realizes the minimum of

$$\gamma \mapsto \sum_{j=0}^J \mathbb{E}[\{Y_{ij}^* - \nu_\gamma(x_i^\top \gamma)\}^2 \mid X_i = x_i]. \quad (8)$$

However, even if m_γ is well defined for any $\gamma \in \mathbb{R}^d$, the vector γ is not identifiable and only its direction could be consistently estimated. Thus, there are two common approaches to restrict γ for identification purposes: either fix one component equal to 1 (Ma and Zhu, 2013), or set the norm of γ equal to 1 and fix the sign of its first component to be positive (Zhu and Xue, 2006). The estimation of the single-index regressions is performed by considering the empirical counterpart of (7) and (8)

$$\hat{\gamma} = \arg \min_{\gamma} \sum_{i=1}^n (\hat{y}_{ij}^* - \hat{\nu}_\gamma(X_i^\top \gamma))^2,$$

$$\hat{y}_{ij}^* = y_{ij} - \frac{1}{n} \sum_{i=1}^n y_{ij}, \quad \text{and} \quad \hat{\nu}_\gamma(u) = \frac{\frac{1}{nh} \sum_{i=1}^n \hat{y}_{ij}^* K\left(\frac{X_i^\top \gamma - u}{h}\right)}{\frac{1}{nh} \sum_{i=1}^n K\left(\frac{X_i^\top \gamma - u}{h}\right)},$$

where K is a kernel and h a bandwidth. The estimation procedure is implemented in the R package **regpro** (Klemela, 2016). The clustering of the regions is also performed on the residuals $\hat{\xi}_i = (\hat{\xi}_{i0}, \dots, \hat{\xi}_{iJ})^\top$ defined by

$$\hat{\xi}_{ij} = \hat{y}_{ij}^* - \hat{\nu}_\gamma(X_i^\top \hat{\gamma}).$$

3.4 Nonparametric clustering of the regions

A wide range of literature focuses on models assuming that, conditionally on knowing the particular cluster the subject i came from, its features are independent (Chauveau et al., 2015). Thus, we consider that the conditional distribution of the $\hat{\xi}_i$ given cluster membership is defined as a product of univariate densities. Note that this assumption imposes non-explicit constraints on the distribution of the noises ε_i defined in (1). Therefore, the clustering of the region is performed by considering the marginal density defined by

$$g(\hat{\xi}_i; \lambda) = \sum_{\ell=1}^L \pi_\ell \prod_{j=1}^J g_{\ell j}(\hat{\xi}_{ij}), \quad (9)$$

where λ groups the mixing proportions π_1, \dots, π_L (where $\pi_\ell > 0$ and $\sum_{\ell=1}^L \pi_\ell = 1$) and the univariate densities $g_{\ell j}$. The model (9) is identifiable, up to a swapping of the cluster labelling, if the densities $g_{\ell j}$ are linearly independent (see Theorem 8 of Allman et al. (2009)). Considering a multivariate kernel defined as a product of J univariate kernels K , the maximum smoothed log-likelihood estimator $\hat{\lambda}$ (MSLE) is obtained by maximizing the smoothed log-likelihood $\ell(\lambda)$ (Levine et al., 2011), such that

$$\hat{\lambda}_L = \arg \max_{\lambda} \ell(\lambda; L)$$

and

$$\ell(\lambda; L) = \sum_{i=1}^n \ln \left\{ \sum_{\ell=1}^L \pi_\ell \prod_{j=1}^J \mathcal{N} g_{\ell j}(\hat{\xi}_{ij}) \right\},$$

where

$$\mathcal{N} g_{\ell j}(\hat{\xi}_{ij}) = \exp \left\{ \int_{\Omega_j} \frac{1}{h_j} K \left(\frac{\hat{\xi}_{ij} - u}{h_j} \right) \ln g_{\ell j}(u) du \right\},$$

and h_1, \dots, h_J are the bandwidths (*i.e.*, $h_j > 0$ and $h_j = o(1)$ for $j = 1, \dots, J$). Considering the MSLE is more convenient than considering the maximum likelihood estimate because the MSLE can be obtained by a Majorization-Minimization algorithm (see Levine et al. (2011) for details on the algorithm and Zhu and Hunter (2016) for recent developments) implemented in the R package **mixtools** Benaglia et al. (2009).

Clustering is achieved by computing the MSLE because this estimator permits a soft assignment where the conditional probability that subject i belongs to cluster ℓ , denoted by $t_{i\ell}(\hat{\lambda})$, can be obtained

$$t_{i\ell}(\hat{\lambda}_L) = \frac{\hat{\pi}_\ell \prod_{j=1}^J \mathcal{N} \hat{g}_{\ell j}(\hat{\xi}_{ij})}{\sum_{\ell'=1}^L \hat{\pi}_{\ell'} \prod_{j=1}^J \mathcal{N} \hat{g}_{\ell' j}(\hat{\xi}_{ij})}.$$

Moreover, a hard assignment can be achieved by applying the maximum *a posteriori* rule (leading that $\hat{z}_{i\ell} = 1$ if $\ell = \arg \max_{\ell'} t_{i\ell}(\hat{\lambda})$ and $\hat{z}_{i\ell} = 0$ otherwise).

4 Numerical experiments

Simulation set-up Data are independently generated from (1), (2) and (6) with $T = 256$, $K = 3$ and unequal proportions such that $Z_i \sim \mathcal{M}(0.5, 0.25, 0.25)$, a function characterizing

class k defined by

$$u_{\ell(t)} = r_{\ell(t)} \mathbf{1}_{\{r_{\ell(t)} > 0\}} \text{ with } r_{\ell(t)} = a_{\ell(t)} \sin \left(b_{\ell} \pi \frac{t}{T} \right),$$

with $a_{1(t)} = 1$, $b_1 = 2.5$, $a_{2(t)} = (1 + \varsigma)$, $b_2 = 2.5$, $a_{3(t)} = (1 + \varsigma \mathbf{1}_{\{t > 128\}})$ and $b_3 = 2.5 - \varsigma$ where $\varsigma = 0.3$. In the attempt to replicate regions' patterns, we devise the three components such that each represents the severity level of COVID-19: moderate throughout, heavy throughout, and moderate during the first wave but drastically more affected in the second wave. Moreover, the lapse between the two waves of the disease is shorter for class 3. We use a heteroscedastic noise defined by $\varepsilon_{ik(1)} \sim \mathcal{N}(0, 0.2^2)$, where the conditional distribution of $\varepsilon_{i\ell(t)} \mid \mathcal{F}_i$, with \mathcal{F}_i the natural filtration, is equal to the conditional distribution of $\varepsilon_{i\ell(t)} \mid \varepsilon_{i\ell(t-1)}$ where

$$\varepsilon_{i\ell(t)} \mid \varepsilon_{i\ell(t-1)} \sim \mathcal{N} \left(0, (0.2 + 0.2\varepsilon_{i\ell(t-1)}^2)^2 \right).$$

The bivariate vector of covariates $X_i = (X_{i1}, X_{i2})^\top$ is composed of two independent standard Gaussian random variables and $\mu(X_i) := \nu(X_i^\top \gamma)$ with $\gamma = [1/\sqrt{2} \ 1/\sqrt{2}]^\top$. To illustrate the benefits of CRFTIW, we consider the following three scenarios, where the first mimics the situation of the COVID-19 daily death curves:

- Scenario 1 (*translations and covariates*): there is a shift and an effect of the covariates since we set $\delta_i = 50$ with probability 0.5 and $\delta_i = 0$ otherwise, and $\nu(a) = (1 + \varsigma(a^2 - 1))$.
- Scenario 2 (*only covariates*): there is no shift but an effect of the covariates since we set $\delta_i = 0$ and $\nu(a) = (1 + \varsigma(a^2 - 1))$.
- Scenario 3 (*only translations*): there is a shift but no effect of the covariates since we set $\delta_i = 50$ with probability 0.5 and $\delta_i = 0$ otherwise, and $\nu(a) = 1$.

For each scenario, we generate 100 replicas by considering three sample sizes: 50, 100 and 250. All nonparametric estimations are done using a Gaussian kernel with a bandwidth $Cn^{-1/5}$ where C represents the empirical standard deviation of the variable considered by the kernel.

Method comparison Results of `CRFTIW` are compared to those of the following methods:

- `depIntra` is similar to `CRFTIW` but clustering is performed by a mixture considering the within component dependencies (Zhu and Hunter, 2019). This model challenges the assumption of a product decomposition of the component densities made in (9).
- `noTI` is similar to `CRFTIW` but the feature extraction is performed with orthogonal wavelets commonly used for wavelet-based clustering (Antoniadis et al., 2013). This model allows to illustrate the advantages of TI wavelets.
- `noCov` is similar to `CRFTIW` but considers that $\mu(x_i) = 1$. This model illustrates the importance of considering the population risk factors.
- `adjustFirst` fits the estimators $(\bar{\mu}, \bar{\gamma})$ of the regression of $\bar{W}_i = \frac{1}{T} \sum_{t=1}^T W_{i(t)}$ on X_i , then uses (9) to cluster the features provided by Step 1 of `CRFTIW` applied on $W_i/\bar{\mu}(x_i^\top \bar{\gamma})$. This model justifies the relevance of the order between Steps 1 and 2 of `CRFTIW`.
- `funFEM` is a standard approach to cluster functional data (Bouveyron et al., 2015) implemented in the R package `funFEM` (Bouveyron, 2015). We use this approach on the curves adjusted with the covariates $W_i/\bar{\mu}(x_i^\top \bar{\gamma})$, a decomposition in a Fourier basis with 25 elements and the arguments of the function `funFEM` are `model='AkjBk'`, `init='kmeans'`, `lambda=0` and `disp=TRUE`. Thus, this model investigates the relevance of the order between Steps 1 and 2 of `CRFTIW`, and the choice of a nonparametric clustering.

Clustering accuracy In all scenarios considered, clustering accuracy of the competing methods is measured using the Adjusted Rand Index (ARI, Hubert and Arabie (1985)) between the estimated partition and the true partition shown in Figure 2. The results show that by considering a more complex model than (9) for clustering is not relevant. Indeed, `CRFTIW` and `depIntra` provide similar results for large samples but `CRFTIW` is more accurate for small samples. Recall that for our COVID-19 study, the sample size is 78 regions and we

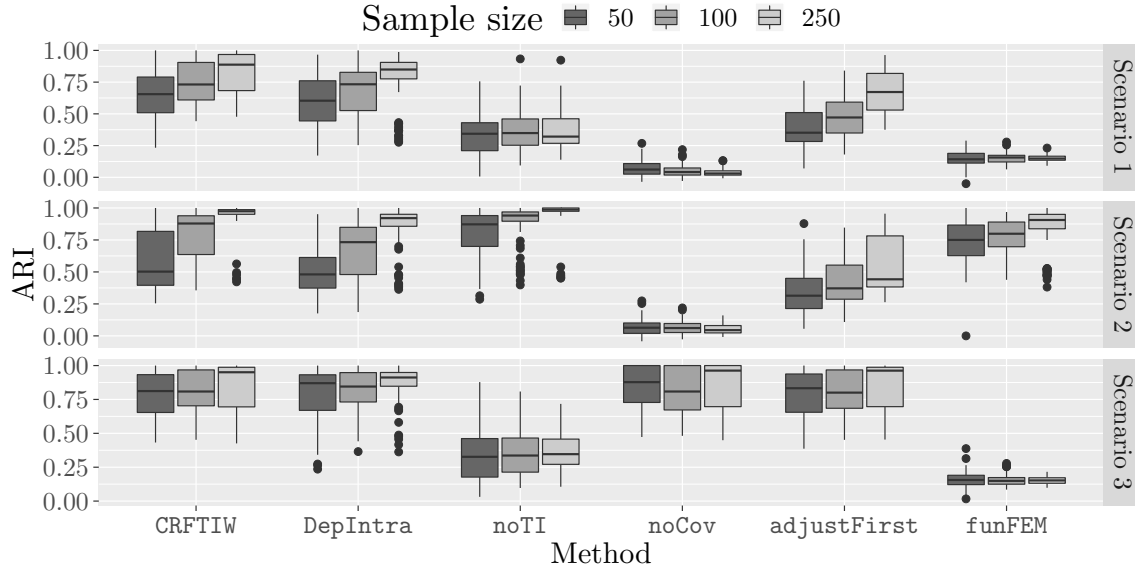


Figure 2: Boxplot of the ARI obtained by the competing methods.

can argue that the model given by (9) is more suitable than a complex model. From Scenarios 1 and 3, the method `noTI` reveals that it is imperative to consider a feature extraction that is invariant to time-shifts. Thus, `CRFTIW` can handle remarkably well situations with different arrival times. When considering the case of population risk factors, such as Scenarios 1 and 2, it is essential to take into account the effects of covariates to fit the partition (see the poor results of `noCov` under these scenarios). Moreover, it seems to be more pertinent to estimate the covariate effects after performing the feature extraction in presence of time-varying arrivals (*i.e.*, `CRFTIW` outperforms `adjustFirst` and `funFEM` under Scenarios 1 and 3).

Covariate effect accuracy The estimation of the covariate effects is a major issue for the COVID-19 application. Indeed, it is essential to properly adjust the covariate effects in order to obtain accurate clusters. Moreover, the parameters and the shape of the function μ make it possible to assert the impact of population risk factors on the death rates. Indeed, the parameters of the index facilitate the interpretation of the population characteristics by distinguishing whether it has a protective or compounding effect. Figure 3(a) shows the dispersion of the estimators of γ_1 around the true value of these parameters, for Scenarios 1

and 2. These results illustrate the consistency of the procedure. Note that, as shown by the results of `adjustFirst`, the accuracy of the regression parameters is slightly better when they are obtained directly from the original data and not from the features given by the wavelet decomposition.

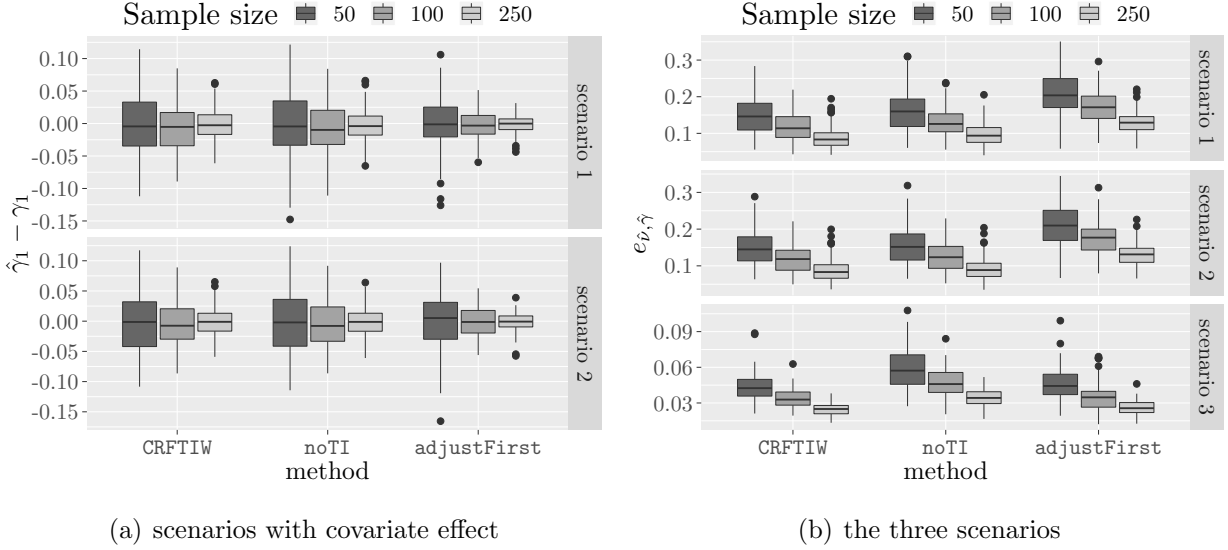


Figure 3: Boxplot of $\hat{\gamma}_1 - \gamma_1$ (a) and $e_{\hat{\nu}, \hat{\gamma}}$ (b) obtained by the competing methods.

Considering two sets of covariates X_i and $X_{i'}$, the difference $\nu(X_i^\top \gamma) - \nu(X_{i'}^\top \gamma)$ can be interpreted as the logarithm of an odds ratio. To investigate the accuracy of the estimator $\hat{\nu}(x_i^\top \hat{\gamma})$, we consider the quantity $e_{\hat{m}, \hat{\gamma}}$ defined by

$$e_{\hat{\nu}, \hat{\gamma}} = \frac{1}{n^2} \sum_{i=1}^n \sum_{i'=1}^n [(\hat{\nu}(x_i^\top \hat{\gamma}) - \hat{\nu}(x_{i'}^\top \hat{\gamma})) - (\nu(x_i^\top \gamma) - \nu(x_{i'}^\top \gamma))]^2.$$

Figure 3(b) depicts the boxplots of $e_{\hat{\nu}, \hat{\gamma}}$ obtained from the three scenarios. Thus, the results reflect the consistency of the approach. Moreover, when there is no effect of the covariates, the convergence of the estimators is much faster. However, in the presence of covariate effects, the accuracy of estimators remains the same with or without a translation. Therefore, we conclude that the translation does not increase the difficulty of the estimation of covariates. Finally, note that despite `adujstFirst` having slightly better parameter estimates, the effects of the covariates (parameters and nonparametric functions) are better estimated with `CRFTIW`.

5 Investigating geographical disparities for COVID-19

The proposed approach allows risk factors to be taken into account. This is a major issue when comparing regions with respect to COVID-19 daily deaths. Indeed, the adjustment on population risk factors enables us to confirm its role (protective or compounding; see Section 5.1). Moreover, this adjustment permits similarities and disparities of the disease impacts to be detected, conditionally on the population characteristics (see Section 5.2). Finally, it allows an *a posteriori* comparison of the clusters with respect to different policy decisions. (*e.g.*, lockdown characteristics; see Section 5.3).

5.1 Population risk factors

The estimated coefficients of the single-index regression are given in Table 1 (row $\hat{\gamma}$). To investigate their significance (*i.e.*, coefficients are not zero), we use an empirical likelihood (EL) approach. Indeed, from Du Roy de Chaumaray et al. (2020), Wilks' theorem holds for the empirical likelihood ratio for semiparametric regressions with weakly dependent data (note that we have $n = 78$ groups of 8 dependent data because each region provides 8 observations used for the coefficient estimation). Thus, we fit the parameters by assuming that one coefficient is zero, then we test the estimated value with the EL approach (see Tests 1-4). Results claim that all the coefficients are significant. All the coefficients in $\hat{\gamma}$ are

Table 1: Estimator of γ obtained considering all coefficients as significant ($\hat{\gamma}$) and estimators obtained assuming that one coefficient is zero (Tests 1-4) with p-value obtained by EL.

	Overweight	Diabetes	Pulmonary	Kidney	p-value
$\hat{\gamma}$	0.626	0.581	0.431	0.291	0.194
Test 1	0.000	0.490	0.611	0.622	0.000
Test 2	0.595	0.000	0.580	0.557	0.000
Test 3	0.693	0.490	0.000	0.529	0.000
Test 4	0.470	0.785	0.403	0.000	0.000

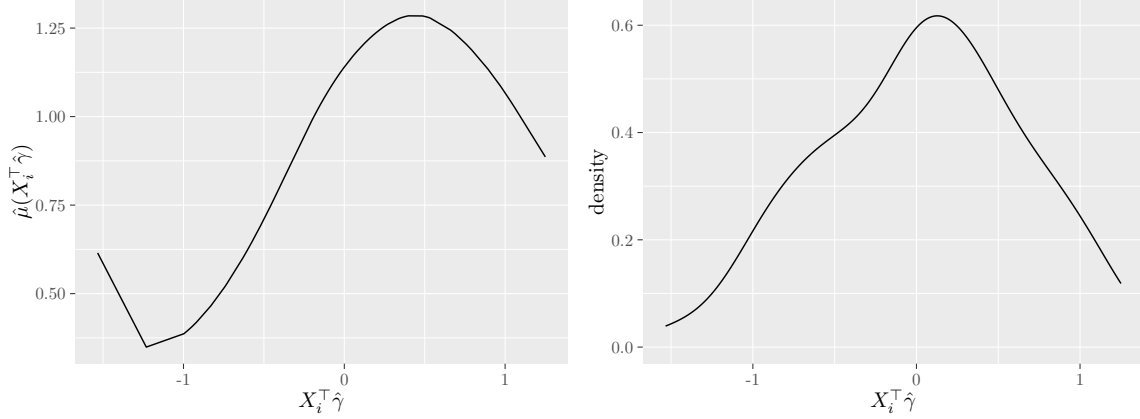


Figure 4: Estimator of the impact of the population risk factors $\hat{\mu}$ (on the left) and density of the index $X_i^\top \hat{\gamma}$ (on the right).

positive. We need to draw the estimated function $\hat{\mu}$ to interpret the impact of these factors on the COVID-19 daily deaths.

Figure 4 shows the estimator of the $\hat{\mu}$ and the density of the index for a range of the index covering 90% of the observed index (this trimming, only performed for this plot, avoids over-interpretation of the curve due to extreme points). This figure confirms that overweight BMI classification, diabetes, COPD and kidney diseases are factors increasing the COVID-19 mortality. These results are in agreement with the main mortality risk factors identified in medical publications (see Zhou et al. (2020, Table 1) and Gupta et al. (2020, Figure 2)). We now illustrate the impact of the adjustment on the population risk factors. Table 2 shows the population risk factors and the index of three regions: France, United Kingdom and Ireland. For example, France and Ireland have a population that is less at risk than the United Kingdom. Taking population risk factors into consideration is vital in order to properly compare the impact of the disease on different regions. Considering the population risk factors is a major key point to compare the impact of the disease on different regions. Figure 5 shows the COVID-19 daily death curves without considering the population risk factors (on the left) and when considering the population risk factors (on the right). Thus, if population characteristics were neglected, one can claim that the first wave of the disease

Table 2: Population risk factors, index and effect of the population risk factors of three regions (France, United Kingdom and Ireland).

Region	Overweight	Diabetes	Pulmonary	Kidney	$X_i^\top \hat{\gamma}$	$\hat{\mu}$
France	1.90	-0.53	-2.02	-1.82	-0.52	0.69
United Kingdom	0.81	-0.71	0.86	-2.02	-0.13	1.05
Ireland	0.27	-0.95	0.50	-1.00	-0.46	0.74

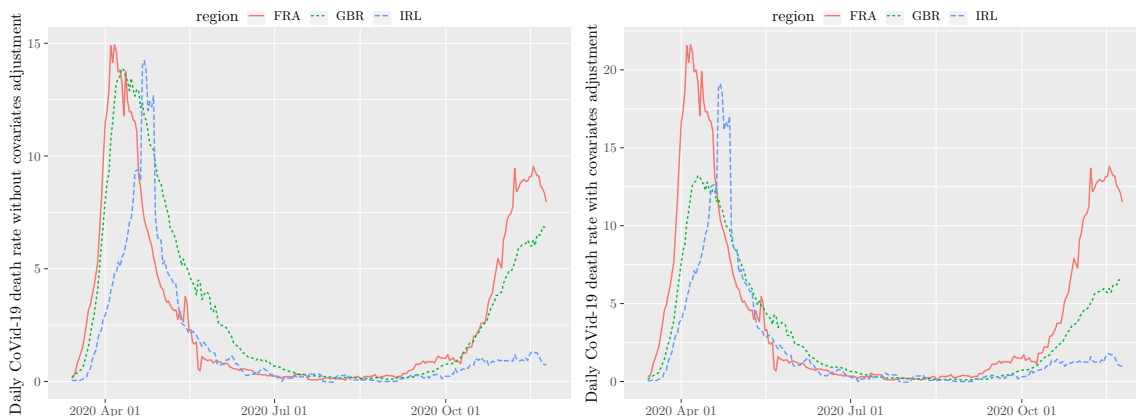


Figure 5: COVID-19 death curves without considering the population risk factors (left) and by considering the population risk factors (right) for France, United Kingdom and Ireland.

(April-May 2020) is similar for these three regions. However, considering the population risk factors, we see that France and Ireland were impacted more greatly than the United Kingdom.

5.2 Clustering of the regions

Clustering is performed by considering a number of clusters between one and ten. Selecting the number of clusters is still a difficult task in nonparametric mixtures. Indeed, despite recent works (Kasahara and Shimotsu, 2014; Kwon and Mbakop, 2020) presenting elegant methods for selecting the number of clusters based on the constraint of linear independence

between the univariate densities required for model identifiability (Allman et al., 2009), these methods require large samples to perform well (see Section 5 of Kwon and Mbakop (2020)). Because we only have 78 regions, we cannot use these methods and thus select the number of clusters by looking for an elbow in the values of the smoothed log-likelihood. These values are presented in Table 3; we focus on the five-clusters partition (note that the difference of $\ell(\hat{\lambda}_L; L)$ obtained with consecutive L is greater than 17 if $L < 5$, otherwise these differences are less than 13; however other number of clusters could be considered).

Table 3: Maximum smoothed log-likelihood $\ell(\hat{\lambda}_L; L)$ with respect to the number of clusters.

L	1	2	3	4	5	6	7	8	9	10
$\ell(\hat{\lambda}_L; L)$	-1034	-894	-815	-791	-774	-767	-754	-743	-733	-734

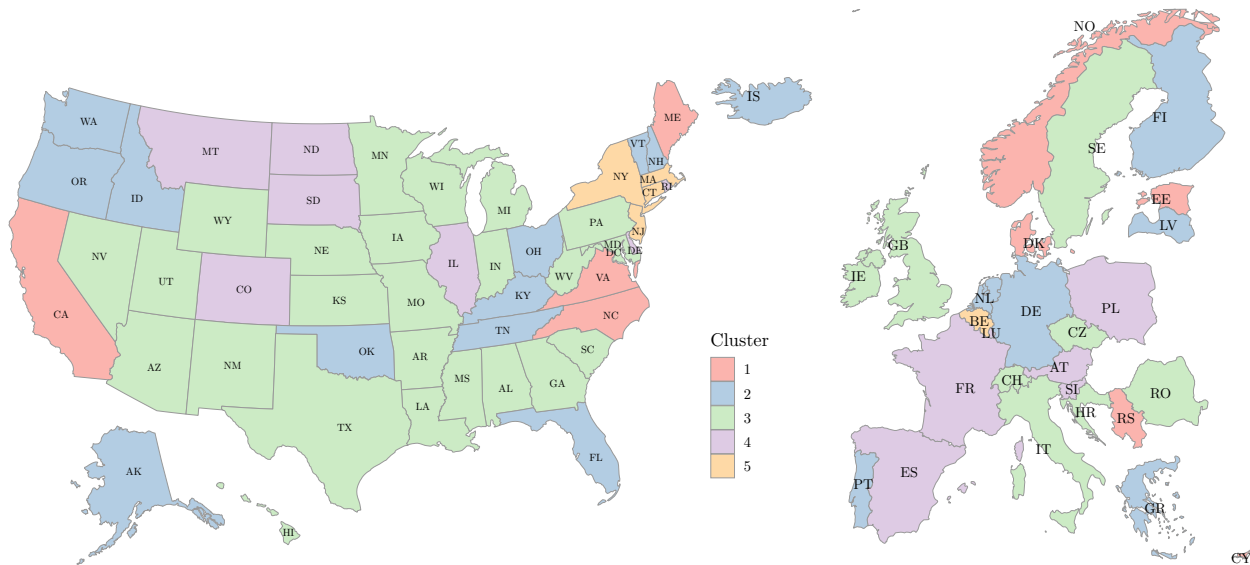


Figure 6: Clustering results.

We now describe the clusters based on summary statistics presented in Table 4 and the curves adjusted with the population risk factors ($W_i/\hat{\mu}(X_i^T \hat{\gamma})$). Figure 6 presents the cluster memberships of each region and Figure 7 presents the curve for one region per cluster and to illustrate our cluster interpretation. The labels of clusters are ordered by the impact of the

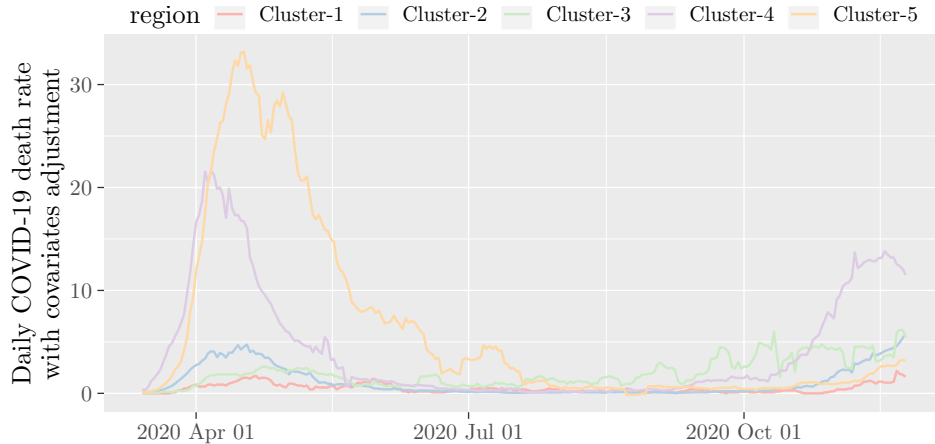


Figure 7: Example of COVID-19 daily death curves adjusted with covariates adjustment $W_{ij}/\hat{\mu}(X_i^\top \hat{\gamma})$. One example per cluster: Maine (Cluster 1), Germany (Cluster 2), Missouri (Cluster 3), France (Cluster 4), New Jersey (Cluster 5).

COVID-19 during the studied period. Thus, cluster 1 has the smallest mean of COVID-19 daily death rates over the studied period and cluster 5 has the highest mean. These results

Table 4: Statistics per cluster

cluster	proportion π_ℓ	Normalized deaths		Covariate effect	
		mean	sd.	mean	sd.
1	0.12	206.88	144.21	0.98	0.28
2	0.25	363.05	155.64	0.87	0.36
3	0.41	636.17	202.51	1.08	0.26
4	0.16	813.50	267.38	0.92	0.28
5	0.07	1314.06	203.31	1.21	0.08

were expected because the distribution of $\hat{\mu}(X_i^\top \hat{\gamma})$ is supposed to be the same among clusters. Clusters can be interpreted, as follows:

- Cluster 1 contains only nine regions that are mainly unaffected from the disease (five countries of EU and four states of USA).

- Cluster 2 contains eighteen regions (seven countries of EU and twelve states of USA) weakly affected by the disease over the whole period except the end where the number of deaths starts to increase.
- Cluster 3 contains 33 regions (eight countries of EU and twenty-five states of USA) moderately impacted by the disease as only one wave of high-death rate is observed.
- Cluster 4 contains thirteen regions strongly impacted by the disease (six countries of EU and seven states of USA). The waves of the high death rate period are characterized by a slow decreasing of the number of deaths when the peak is reached.
- Cluster 5 contains five regions dramatically impacted by the disease (Belgium and four states of USA) especially during the first wave of the disease whose peak is characterized by an abrupt increase of the rate of death.

5.3 Clusters analysis example: disparities and policy decisions

Amid unforeseen difficulties related to COVID-19, policymakers have resorted to various interventions in attempts to curb the spread of the coronavirus. As seen in Sections 5.1 and 5.2, by adjusting the risk factors, the proposed approach allows us to detect vulnerable regions and compare them fairly. Additionally, the homogeneity within cluster enables us to analyze the disparities in factors between clusters; for instance, in this paper, we are looking at the government responses. Note that one may also be interested to study the COVID-19's impact on the population mental health or the economic indicators.

Figure 8(a) shows the distribution of the value for each indicator, *i.e.*, containment health, government response and stringency, with respect to its clusters. As we observe, the difference between the first four clusters is not noticeable for each indicator, but the indicators take larger values for regions of cluster 5 (containing the most impacted regions). The same phenomenon is observed for the specific measures adopted by the governments presented in Figure 8(b).

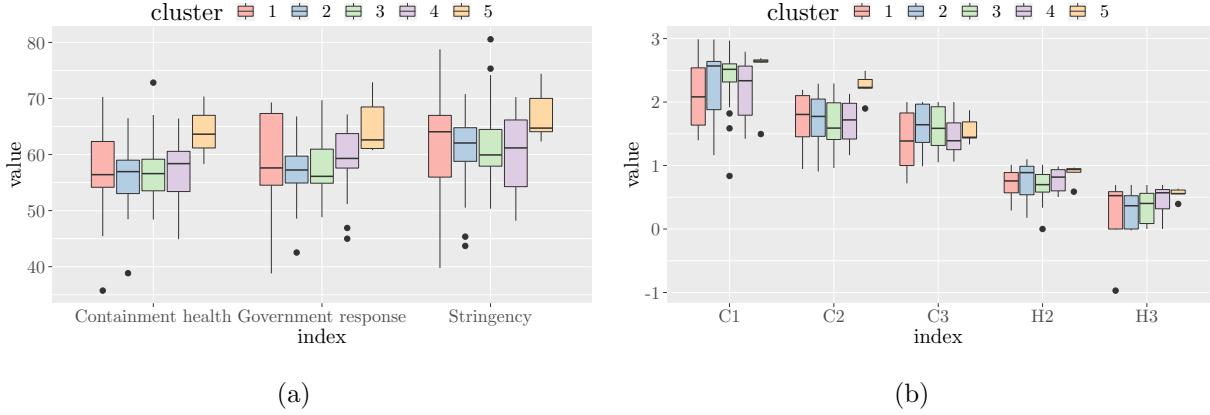


Figure 8: Boxplot of the overall indicator values for each cluster (a) and for specific measures adopted for each cluster (b): School closing (C1), Workplace closing (C2), Cancel public events (C3), Testing policy (H2) and Contact tracing (H3).

Cluster 5, which was strongly affected by the virus, seems to take more stringent measures than the other regions. One plausible explanation is that the policymakers may abruptly enforce restrictive countermeasures in hopes to lower the increasing mortality rate, thus the observed steep descent. Hence, the effectiveness of government response may depend on the timing of the measure’s implementation, the duration and the stringency (Cheng et al., 2020; Haug et al., 2020). To further understand the relationship between the mortality rate and the various policies adopted in reaction to the COVID-19, a more precise analysis can be achieved by fitting a model for multivariate non-stationary time series per clusters (the time series being the daily death rate and the index mentioned above). Thus, a description of the relation between the government responses and the COVID-19 death curve can be done using the model parameters. This can be achieved by modelling the dependencies between the time series (Molenaar et al., 1992; Sanderson et al., 2010) or by a multiple change-point detection (Cho and Fryzlewicz, 2015). Moreover, a comparison of the government interventions to COVID-19 can be conducted by comparing the models fitted for each cluster.

6 Conclusion

This paper introduces **CRFTIW**, a new method to cluster functional data when observations are shifted and external covariates are allowed to have a scale effect. **CRFTIW** is a three-step approach developed for the purpose of analyzing geographical disparities of the COVID-19 impact (measured by the daily number of deaths per million people).

As a first step of **CRFTIW**, feature extraction is performed with TI wavelets. While providing an adapted and compact representation of the data, it also permits us to deal with the different times of arrivals of the disease. The main limitation of this approach lies in the dyadic data constraint of the considered sample. This issue could be overcome, for example, by using second generation wavelets and in particular the lifting scheme (Sweldens (1998)), but would lose the property of translation-invariance. However, extending this construction, while preserving both the property of translation-invariance and the property of conservation of the norm of the coefficients, seems to be an open question that we leave for future work.

As a second step of **CRFTIW**, the effect of the population risk factors on the extracted feature is estimated and thus regions can be compared as if they have the same sensitivity of the population to the disease. This step is crucial because we aim to investigate the impact of policy decisions. Obviously, if the purpose is to investigate geographical disparities of the impact of the disease, then no adjustment on the population risk factors should be considered. In such case, **CRFTIW** can still be used by considering $\mu(X_i^T \gamma) = 1$. In the analysis of COVID-19, we consider four main factors of comorbidity (overweight, diabetes, chronic pulmonary and kidney diseases). These factors are well-known to increase the risk of COVID-19 mortality, (Zhou et al., 2020; Gupta et al., 2020) and Wilks' theorem for the empirical likelihood permits us to conclude on the significance of the estimated coefficients. However, we advise considering factors already known to be compounded for the disease, and not to use **CRFTIW** to investigate the impact of population risk factors. Indeed, **CRFTIW** does not perform variable selection of the population risk factors and does not permit concluding on causality of the factors.

As a third step of CRFTIW, a nonparametric mixture is used to achieve the clustering with the assumption that the density of the component is defined as a product of univariate densities. Numerical experiments presented in the paper suggested that considering a more complex model deteriorated the results when the sample size is small (like in the COVID-19 application). However, if the data to be analyzed are composed of several observations, more advanced models could be used (Mazo and Averyanov, 2019; Zhu and Hunter, 2019).

Through the COVID-19 dataset, we had illustrated the importance of adjusting the population risk factors, allowing us to compare regions with a ‘standard’ comorbidity. Thus, CRFTIW found five clusters justified by the mortality rate and curvature. Regions within clusters are varied geographically with different onsets, validating the property of translation-invariance of the proposed method. In addition, as we illustrated, investigations on the effectiveness and agility of government response, the consequences on economic indicators or the impact on human mental health, could be achieved by studying disparities of the indicators between clusters.

Driven by the COVID-19 dataset, we developed this novel approach. However, its application is not limited only to COVID-19. For instance, the problem of time-shifts is also observed in electrocardiogram heartbeat, which Annam et al. (2011) tackle when clustering heartbeat abnormalities. Our approach could not only handle the time-shift issue, but also allow for adjusting with regards to plausible factors that may influence the heart-beat. Further, this could extend beyond medical settings: in motion capture (Li and Prakash, 2011), there is interest in categorizing types of motion. This could be used for fitness applications to identify whether a person is running or walking, where the motions may begin at different times on separate observed sequences showing a need for the TI property. Since motion can come from different participants, covariate adjustment could also be beneficial for such data.

References

Allman, E. S., Matias, C., and Rhodes, J. A. (2009). Identifiability of parameters in latent structure models with many observed variables. *The Annals of Statistics*, 37:3099–3132.

- Annam, J. R., Mittapalli, S. S., and Bapi, R. S. (2011). Time series clustering and analysis of ecg heart-beats using dynamic time warping. In *2011 Annual IEEE India Conference*, pages 1–3.
- Antoniadis, A., Brossat, X., Cugliari, J., and Poggi, J.-M. (2013). Clustering functional data using wavelets. *Int. J. Wavelets Multiresolution Inf. Process.*, 11:1350003.
- Attaway, A., Zein, J., and Hatipoglu, U. (2020). Sars-cov-2 infection in the copd population is associated with increased healthcare utilization: An analysis of cleveland clinic’s covid-19 registry. *EClinicalMedicine*, 26:100515.
- Badr, H. S., Zaitchik, B. F., Kerr, G. H., Colston, J. M., Hinson, P., Chen, Y., Nguyen, N. H., Kosek, M., Du, H., Dong, E., Marshall, M., Nixon, K., and Gardner, L. M. (2020). Unified covid-19 dataset. https://github.com/CSSEGISandData/COVID-19_Unified-Dataset.
- Barron, E., Bakhai, C., Kar, P., Weaver, A., Bradley, D., Ismail, H., Knighton, P., Holman, N., Khunti, K., Sattar, N., Wareham, N., Young, B., and Valabhji, J. (2020). Associations of type 1 and type 2 diabetes with covid-19-related mortality in england: A whole-population study. *The Lancet Diabetes Endocrinology*, 8:813–822.
- Benaglia, T., Chauveau, D., Hunter, D., and Young, D. (2009). mixtools: An r package for analyzing finite mixture models.
- Berkner, K. and Wells Jr., R. O. (2002). Smoothness estimates for soft-threshold denoising via translation-invariant wavelet transforms. *Appl. Comput. Harmon. Anal.*, 12:1–24.
- Bouveyron, C. (2015). funfem: clustering in the discriminative functional subspace.
- Bouveyron, C., Côme, E., and Jacques, J. (2015). The discriminative functional mixture model for a comparative analysis of bike sharing systems. *Ann. Appl. Stat.*, 9:1726–1760.
- Center for Disease Control and Prevention (2020). Data & statistics. available at <https://www.cdc.gov/DataStatistics>.

- Chauveau, D., Hunter, D. R., and Levine, M. (2015). Semi-parametric estimation for conditional independence multivariate finite mixture models. *Statistics Surveys*, 9:1–31.
- Cheam, A. S. and Fredette, M. (2020). On the importance of similarity characteristics of curve clustering and its applications. *Pattern Recognition Letters*, 135:360 – 367.
- Chen, J., Yan, J., and Zhang, P. (2020). Clustering us states by time series of covid-19 new case counts with non-negative matrix factorization.
- Cheng, C., Barceló, J., Hartnett, A., Kubinec, R., and Messerschmidt, L. (2020). Covid-19 government response event dataset (corononet v.1.0). *Nat. Hum. Behav.*, 4:756–768.
- Cho, H. and Fryzlewicz, P. (2015). Multiple-change-point detection for high dimensional time series via sparsified binary segmentation. *J. R. Stat. Soc. Ser. B Methodol.*, pages 475–507.
- Coifman, R. R. and Donoho, D. L. (1995). *Translation-invariant de-noising*, pages 125–150. Springer New York, New York, NY.
- Daubechies, I. (1992). *Ten lectures on wavelets*, volume 61. Siam.
- Du Roy de Chaumaray, M., Marbac, M., and Patilea, V. (2020). Wilks’ theorem for semi-parametric regressions with weakly dependent data.
- Ferraty, F. and Vieu, P. (2006). *Nonparametric functional data analysis*. Springer Series in Statistics, New York.
- Global Burden of Disease Collaborative Network (2020). The global health data exchange. <http://ghdx.healthdata.org/gbd-results-tool>. Seattle, United States.
- Gupta, S., Hayek, S. S., Wang, W., Chan, L., Mathews, K. S., Melamed, M. L., Brenner, S. K., Leonberg-Yoo, A., Schenck, E. J., Radbel, J., et al. (2020). Factors associated with death in critically ill patients with coronavirus disease 2019 in the us. *JAMA Intern. Med*, 180:1436–1446.

- Hall, P. and Zhou, X.-H. (2003). Nonparametric estimation of component distributions in a multivariate mixture. *The Annals of Statistics*, 31:201–224.
- Haug, N., Geyrhofer, L., Londei, A., Dervic, E., Desvars-Larrive, A., Loreto, V., Pinior, B., Thurner, S., and Klimek, P. (2020). Ranking the effectiveness of worldwide covid-19 government interventions. *Nat. Hum. Behav.*, 4:1303–1312.
- Holman, N., Knighton, P., Kar, P., O’Keefe, J., and Curley, M. (2020). Risk factors for covid-19 related mortality in people with type 1 and type 2 diabetes in england: a population-based cohort study. *Lancet Diabetes Endocrinology*, 8:823–833.
- Hubert, L. and Arabie, P. (1985). Comparing partitions. *Journal of Classification*, 2:193–218.
- Jacques, J. and Preda, C. (2014). Functional data clustering: a survey. *Advances in Data Analysis and Classification*, 8:231–255.
- Kang, Z., Luo, S., Gui, Y., Zhou, H., Zhang, Z., Tian, C., Zhou, Q., Wang, Q., Hu, Y., Fan, H., and Hu, D. (2020). Obesity is a potential risk factor contributing to clinical manifestations of covid-19. *International Journal of Obesity*, 44:2479–2485.
- Kasahara, H. and Shimotsu, K. (2014). Non-parametric identification and estimation of the number of components in multivariate mixtures. *J. R. Stat. Soc. Ser. B Methodol.*, pages 97–111.
- Klemela, J. (2016). regpro: Nonparametric regression. R package version 0.1.1.
- Kwon, C. and Mbakop, E. (2020). Estimation of the number of components of non-parametric multivariate finite mixture models. *Annals of Statistics (to appear)*.
- Levine, M., Hunter, D. R., and Chauveau, D. (2011). Maximum smoothed likelihood for multivariate mixtures. *Biometrika*, 18:403–416.
- Li, L. and Prakash, B. A. (2011). Time series clustering: Complex is simpler! In *ICML*.

- Liang, H., Liu, X., Li, R., and Tsai, C.-L. (2010). Estimation and testing for partially linear single-index models. *Ann. Statist.*, 38(6):3811–3836.
- Ma, Y. and Zhu, L. (2013). Doubly robust and efficient estimators for heteroscedastic partially linear single-index model allowing high-dimensional covariates. *J. R. Stat. Soc. Ser. B Methodol.*, 75:305–322.
- Mallat, S. G. (1989). A theory for multiresolution signal decomposition: the wavelet representation. *IEEE transactions on pattern analysis and machine intelligence*, 11:674–693.
- Mallat, S. G. (2008). *A wavelet tour of signal processing: the sparse way*. Academic press.
- Mazo, G. and Averyanov, Y. (2019). Constraining kernel estimators in semiparametric copula mixture models. *Computational Statistics & Data Analysis*, 138:170–189.
- McLachlan, G. J. and Peel, D. (2004). *Finite mixture models*. John Wiley & Sons.
- Molenaar, P. C., De Gooijer, J. G., and Schmitz, B. (1992). Dynamic factor analysis of nonstationary multivariate time series. *Psychometrika*, 57(3):333–349.
- Navarro, F. and Chesneau, C. (2020). R package rwavelet: Wavelet analysis. *Version 0.4.1*.
- Owen, A. B. (2001). *Empirical likelihood*. Chapman and Hall/CRC.
- Qin, J. and Lawless, J. (1994). Empirical likelihood and general estimating equations. *The Annals of Statistics*, 22:300–325.
- Ramsay, J. O. and Silverman, B. W. (2007). *Applied functional data analysis: methods and case studies*. Springer.
- Sanderson, J., Fryzlewicz, P., and Jones, M. (2010). Estimating linear dependence between nonstationary time series using the locally stationary wavelet model. *Biometrika*, 97(2):435–446.
- Severini, T. A. and Wong, W. H. (1992). Profile likelihood and conditionally parametric models. *The Annals of Statistics*, 20:1768–1802.

- Sweldens, W. (1998). The lifting scheme: A construction of second generation wavelets. *SIAM Journal on Mathematical Analysis*, 29:511–546.
- Tang, C., Wang, T., and Zhang, P. (2020). Functional data analysis: An application to covid-19 data in the united states.
- Unser, M. (1995). Texture classification and segmentation using wavelet frames. *IEEE Transactions on Image Processing*, 4:1549–1560.
- Wang, K. and Gasser, T. (1997). Alignment of curves by dynamic time warping. *The Annals of Statistics*, 25:1251–1276.
- Williamson, E., Walker, A., Bhaskaran, K., et al. (2020). Factors associated with covid-19-related death using opensafely. *Nature*, 584:430–436.
- World Health Organization (2016). Icd-10 : International statistical classification of diseases and related health problems : tenth revision.
- World Health Organization (2020). The global health observatory. <https://www.who.int/data/gho/data/indicators>.
- Zhou, F., Yu, T., Du, R., Fan, G., Liu, Y., Liu, Z., Xiang, J., Wang, Y., Song, B., Gu, X., Guan, L., Wei, Y., Li, H., Wu, X., Xu, J., Tu, S., Zhang, Y., Chen, H., and Cao, B. (2020). Clinical course and risk factors for mortality of adult inpatients with covid-19 in wuhan, china: A retrospective cohort study. *The Lancet*, 395:1054–1062.
- Zhu, L. and Xue, L. (2006). Empirical likelihood confidence regions in a partially linear single-index model. *J. R. Stat. Soc. Ser. B Methodol.*, 68:549–570.
- Zhu, X. and Hunter, D. R. (2016). Theoretical grounding for estimation in conditional independence multivariate finite mixture models. *J. Nonparametr. Stat.*, 28:683–701.
- Zhu, X. and Hunter, D. R. (2019). Clustering via finite nonparametric ica mixture models. *Advances in Data Analysis and Classification*, 13:65–87.

A Proof of Lemma 1

Proof of Lemma 1. We consider the matrix representation for the discrete wavelet transform. For the orthogonal case, the discrete transform of a vector $w \in \mathbb{R}^T$ is represented by an $T \times T$ orthogonal matrix M (see, *e.g.*, Mallat (2008)).

$$M = \begin{pmatrix} \phi(1) & \psi_{0,0}(1) & \dots & \psi_{J-1,2^{J-1}}(1) \\ \vdots & \vdots & & \vdots \\ \phi(T) & \psi_{0,0}(T) & \dots & \psi_{J-1,2^{J-1}}(T) \end{pmatrix}^\top.$$

In the translation-invariant case, the downsampling of the locations k is discarded at each scale j , and the decomposition can thus be written as follows

$$W_i(t) = \sum_{k=0}^{T-1} \alpha_{i,0,k} \phi_{0,k}(t) + \sum_{j=0}^{J-1} \sum_{k=0}^{T-1} \beta_{i,j,k} \psi_{j,k}(t), \quad t \in [1, T], \quad i = 1, \dots, n.$$

The matrix representation is therefore given by an $(J+1)T \times T$ matrix M which corresponds to the row-wise concatenation of the J , $T \times T$ matrices which yield the wavelet coefficients at scale j plus the matrix which produces the scaling coefficients (see, *e.g.*, Berkner and Wells Jr. (2002); Coifman and Donoho (1995) for a full representation, in terms of filters). The representation at scale j for W_i given z_i is defined by $M_j W_i$ where M_j denotes either the $T \times 2^j$ or the $T \times T$ wavelet transform matrix at scale j , for $j = 0, \dots, J$. Thus, we have

$$M_j W_i = \sum_{\ell=1}^L z_{i\ell} M_j \left[\mu(x_i) (u_\ell^{(\delta_i)} + \varepsilon_{i\ell}^{(\delta_i)}) \right].$$

Therefore, the logarithm of the total energy at scale j for W_i given z_i is given by

$$y_{ij} = \ln \left(\mu^2(x_i) \sum_{\ell=1}^L z_{i\ell} \|v_{\ell j} + \varepsilon_{i\ell j}^*\|_2^2 \right) = \ln \mu(x_i) + \frac{1}{2} \ln \left[\sum_{\ell=1}^L \pi_\ell \|v_{\ell j} + \varepsilon_{i\ell j}^*\|_2^2 \right],$$

where $v_{\ell j} = M_j u_\ell^{(\delta_i)}$ and $\varepsilon_{i\ell j}^* = M_j \varepsilon_{i\ell}^{(\delta_i)}$. Considering the centered version of the elements leads to (5). Noting that the noise of the regression follows a mixture model where the latent variable is z_i (*i.e.*, the same latent variable that the one use to defined the marginal distribution of W_i), permits to conclude that clustering the noise of the regression obtained

for the different scale is relevant to cluster the curves W_i . Finally, noting that by assumption X_i is independent to Z_i and $\varepsilon_{i\ell}$ and that $\varepsilon_{i\ell j}^*$ is defined as a combination of the original $\varepsilon_{i\ell}$ permits to concluded on the independence between X_i and $\varepsilon_{i\ell j}^*$.

□